Audio Engineering Society

Convention Paper

Presented at the 120th Convention
2006 May 20–23 Paris, France

Enhanced control of sound field radiated by co-axial loudspeaker systems using Digital Signal Processing techniques

Hmaied Shaiek[1], Bernard G.A. Debail[2], Jean Marc Boucher[1], Yvon Kerneis[2] and Pierre Yves Diquelou[2]

[1] *GET, ENST Bretagne Département SC, CNRS TAMCIC, Technopôle Brest-Iroise - CS 83818 29238 Brest Cedex 3, France*

[2] *Cabasse Acoustic Center, Plouzané, 29280, France*

Correspondence should be addressed to Hmaied, Bernard (`hmaied.shaiek@enst-bretagne.fr`, `bernard.debail@cabasse.com`)

ABSTRACT

In multi-way loudspeaker systems, digital signal processing techniques have been used so far mainly to correct frequency response, time alignment and out of axis lobbing. In this paper, a new signal processing technique is described in order to also control the sound field radiated by co-axial loudspeaker systems in the overlap frequency band of drivers. Trades-off and practical constraints (crossover, time shift, gain...) are discussed and an optimization algorithm is proposed to provide the best achievable result. Real-time implementation of this technique is presented and leads to a nearly ideal point source.

1. INTRODUCTION

In a previous paper [1], the advantages of a co-axial distribution have been demonstrated in terms of sound field radiation, lobbing and phase shift deviation compared to a traditional discrete geometrical distribution of transducers. However, due to practical constraints, some less significant imperfections in terms of sound radiation still remain.

In a co-axial loudspeaker system, a prefect co-incidence of driver acoustic centers is hard to achieve. That's why the respective impulse responses are slightly delayed. Additionally, the sound field radiated by the system is highly influenced by crossover filter transfer functions in transducer overlap regions. Thus, special care must be taken when choosing filter slopes or cut-off frequencies.

The purpose of this paper is to describe a Digital Signal Processing technique especially appropriated

to co-axial configuration that counteracts the previous defects. Firstly, this technique consists in finding the suitable delay to be applied to each way in order to obtain nearly co-incident transducers. Secondly a dedicated linear-phase crossover is designed to achieve good driver's separation. This crossover will then be optimized over the cut-off bands in order to achieve better radiation characteristics. Thirdly, a suitable linear-phase equalizer will be included to correct the system response on-axis or over 30 degrees solid angle. Finally, the overall processing described will be implemented on Analog Devices (AD) $ADSP-21262$ device, a 32-bit floating point DSP dedicated to professional audio applications.

2. PROPOSED CO-AXIAL SYSTEM

In this paper, we will consider the acoustic source introduced in [1]. It's a three-way co-axial loudspeaker dedicated to the reproduction of the frequency band: $[80Hz, 20kHz]$. The terminology used for the different driver is the following:

- $Low-mid$: low medium frequencies reproduction $80Hz \leq f \leq 1000Hz$.
- $Upper-mid$: high medium frequencies reproduction $500Hz \leq f \leq 5000Hz$.
- $Tweeter$: high frequencies reproduction $3000Hz \leq f \leq 22000Hz$.

The Tweeter is a disc of diameter $d_{tw} = 28mm$ surrounded by the Upper-mid concentric radiating ring with an outside diameter of $d^o_{um} = 106mm$ and inside diameter of $d^i_{um} = 43mm$. The previous drivers constitute the $BC13$ unit mounted inside the Low-mid ring with an outside diameter of $d^o_{lm} = 204mm$ and an inside diameter of $d^i_{lm} = 124mm$.

We consider that the three-way co-axial loudspeaker will be referenced into space in a Cartesian coordinate with the symbols depicted in figure 1.

The signal processing technique proposed in the following will be applied to this loudspeaker realization. However, this method can be extended to any equivalent co-axial system

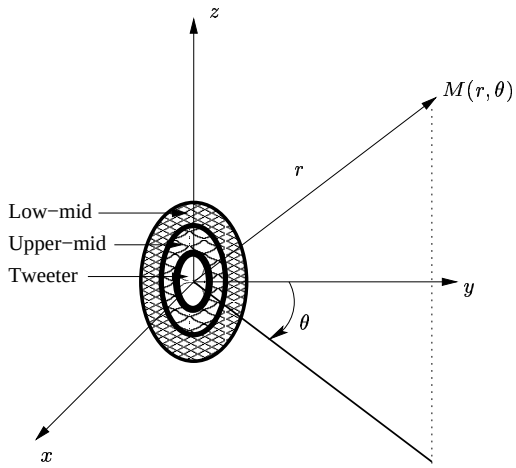

Fig. 1: Three-way co-axial loudspeaker in a Cartesian coordinate

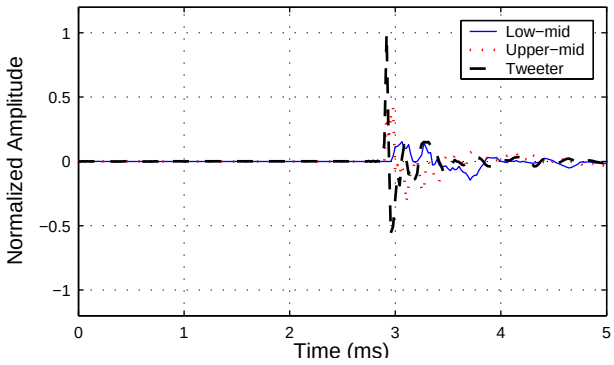

Fig. 2: On-axis transducer impulse responses

3. DRIVER SYNCHRONIZATION

During the design of the co-axial source, the membranes have been deliberately placed one behind the other in order to provide a free field radiation of the sound wave and limit diffraction effects as illustrated on figure **??**. This induces slight shifts between driver acoustic centers along the central axis as confirmed by the impulse response of individual drivers depicted on figure 2.

These delays are equivalent to $d_{tu} = 1.42cm$ respectively $d_{ul} = 2.13cm$ of physical separation between the Tweeter and the Upper-mid device, respectively between the Upper-mid and the Low-mid device.

The impact of this technical constraint on the sound

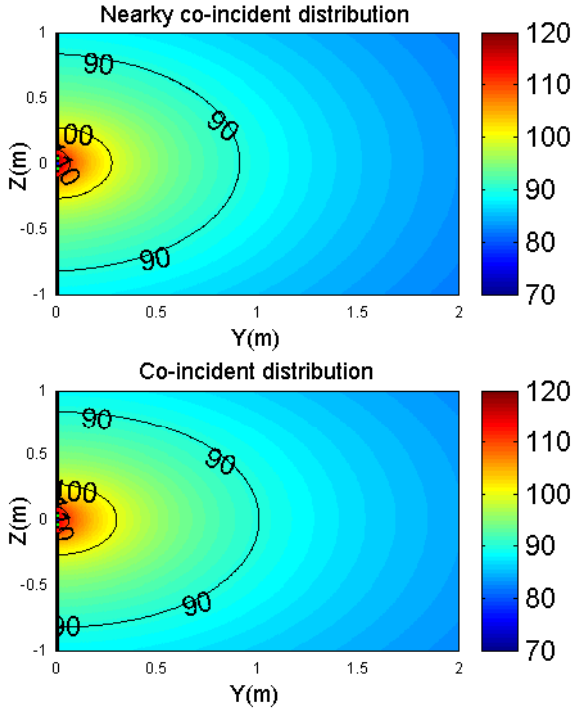

Fig. 3: Simulated $2D$ plot of the radiated field of co-incident and nearly co-incident co-axial loudspeaker on the (Oy, Oz) plane at $800Hz$

field radiated by the three-way co-axial loudspeaker model proposed in [1] is given by figure 3 and 4. These figures display some $2D$ map description of the radiating field in the (Oy, Oz) plane at two crossover frequencies $f_1 = 800Hz$ and $f_2 = 4500Hz$ [1]. For the co-incident system, the membranes are co-planar. However for the nearly co-incident one, the membranes are shifted by d_{tu} and d_{ul}.

At $f_1 = 800Hz$, the two sources are radiating a nearly perfect spherical wave of an ideal monopole with a $1/r$ magnitude decrease. However, at $f_2 = 4500Hz$, the nearly co-incident source starts to slightly steer on-axis but the radiation pattern remains extremely homogeneous even in near field.

In [2], Fink proposed the compensation of axial delays using analog filters. However, using digital techniques, these time-shifts could be easily corrected

[1] For a detailed description of the acoustical model used for the simulations the reader can refer to [1].

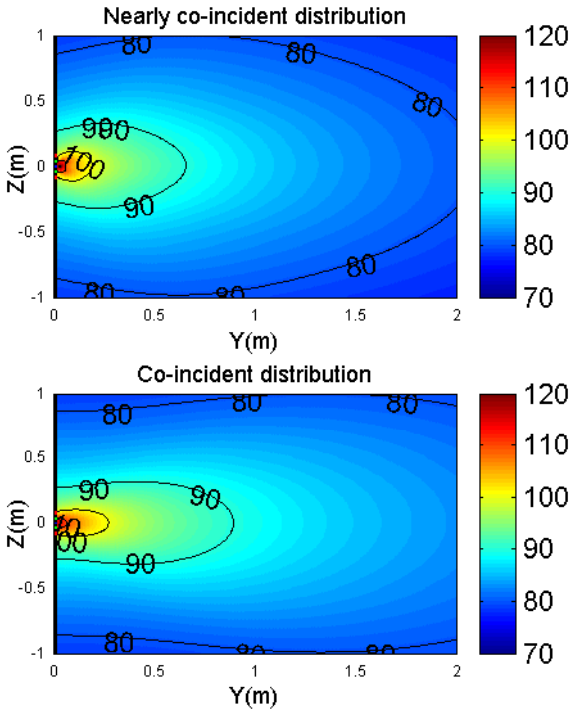

Fig. 4: Simulated $2D$ plot of the radiated field of co-incident and nearly co-incident co-axial loudspeaker on the (Oy, Oz) plane at $4500Hz$

using simple delay lines that will be then included in the crossover design.

4. DIGITAL CROSSOVER FILTERS

4.1. Structure and design method

The structures and design methods of crossover filters were largely discussed in the literature [3], [4], [6] and [7]. It was retained unanimously that transverse linear phase structures are the best adapted for the synthesis of these filters. Indeed, they allow an easy synthesis of flat overall amplitude response (no additional deviation) as well as, linear phase behavior (which correspond to pure and controllable delay). Additionally, this filter structure is always stable which is a suitable criterion for real-time implementation.

The window method was adopted for the synthesis of crossover filters [3]. It corresponds to a weighting (by a Kaiser window) of the truncated impulse response of a target filter obtained from a target frequency response.

When filters have different lengths, the overall crossover response shows amplitude notches around overlap frequencies due to unequal group delays. We can easily overcome this problem by introducing extra delays [8] through the ways in advance. For two linear phase filters of N_1 and N_2 taps (with $N_1 > N_2$) and working at f_s sampling frequency, this delay is:

$$\tau = \frac{N_1 - N_2}{2f_s} \tag{1}$$

In order to enhance the loudspeaker protection and cut-off extremely low and high frequencies, additional high-pass (cutting at $100Hz$ and having $12dB/oct$ slope) and low-pass (cutting at $20kHz$ and having $48dB/oct$ slope) were included. The crossover is thus a bank of three linear phase band-pass filters ($L_0(z)$, $U_0(z)$ and $T_0(z)$) cascaded with suitable delays (z^{-L_1} and z^{-L_2}) to ensure equal group delay filters and synchronous drivers. A block diagram of the filter bank is given by figure 5.

Crossover filter transfer functions will be written as follow:

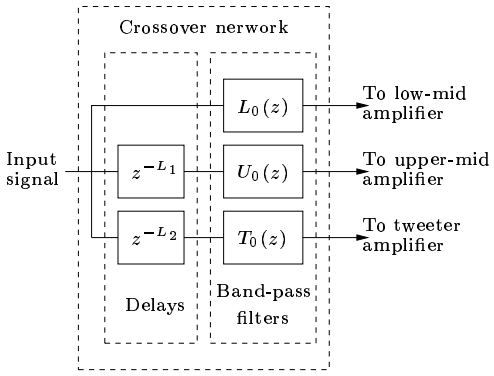

Fig. 5: Block diagram of the crossover network

$$\begin{aligned} L_1(z) &= L_0(z) \\ U_1(z) &= z^{-L_1}U_0(z) \\ T_1(z) &= z^{-L_2}T_0(z) \end{aligned} \tag{2}$$

4.2. Definition: overlap band

The frequency band in which two transducers contribute simultaneously to the radiated field is the overlap band. In figure 6, we can see that the three-way co-axial loudspeaker have following overlap bands:

- $Low - mid/Upper - mid$: for $300Hz \leq f \leq 1500Hz$.
- $Upper - mid/Tweeter$: for $2000Hz \leq f \leq 7000Hz$.

Crossover filter parameters (cut-off frequencies and slopes) must be chosen subject to these overlap bands.

4.3. Radiation characteristics

Taking into account the symmetry of revolution of the membranes of the co-axial system and the quasi-coincidence of the three acoustic centers, we can write that the transfer function of the filtered system in a point $M(r,\theta)$ of the space is:

$$\begin{aligned} H_{sys}(r,\theta,f) &= H_{lm}(r,\theta,f)L_1(f) \\ &+H_{um}(r,\theta,f)U_1(f) + H_{tw}(r,\theta,f)T_1(f) \end{aligned} \tag{3}$$

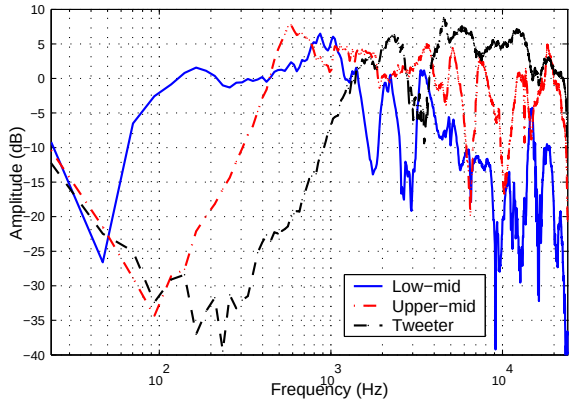

Fig. 6: On-axis transducer frequency responses of the three-way co-axial loudspeaker

Where, $H_{lm}(r,\theta,f)$, $H_{um}(r,\theta,f)$ and $H_{tw}(r,\theta,f)$ are the transfer functions of the low-mid, upper-mid and tweeter device.

The on-axis response of the system is:

$$H_{ax}(r,f) = H_{sys}(r,0,f) = H_{lm}(r,0,f)L_1(f) + H_{um}(r,0,f)U_1(f) + H_{tw}(r,0,f)T_1(f) \quad (4)$$

Assuming a spherical wave radiation with an $1/r$ magnitude decrease, the directional factor F of the source [5] is given by:

$$F(\theta,f) = \left| \frac{H_{sys}(r,\theta,f)}{H_{ax}(r,f)} \right| \quad (5)$$

The variation of the intensity level (or sound pressure level) with angle is the radiation pattern of the source and is given by:

$$R(\theta,f) = 20log10(F(\theta,f)) \quad (6)$$

The directivity of the acoustic source (see Appendix) can be approached by:

$$D(f) = \frac{2}{\int_0^{\pi}(F(\theta,f))^2 sin(\theta)d\theta} \quad (7)$$

The directivity index is then given by:

$$DI(f) = 10log10(D(f)) \quad (8)$$

From the previous equations, we can see that the loudspeaker radiation characteristics are function of crossover filter transfer functions especially over the overlap bands.

4.4. Choice of filter cut-off frequencies

4.5. Low-mid / upper-mid cut-off frequency

The choice of the correct cut-off frequencies is determined by several characteristics. As far as, the low-mid driver is concerned, the maximum frequency is limited by the occurring of modes of the membranes and directivity lobbing. For the upper-mid side, the minimum frequency is limited by the ability of this drive unit to reproduce flat frequency response at reasonable high power level without audible distortions. The cut-off frequency should be chosen in such a way that the directivity pattern of the two drive-units are pretty similar. This leads to a cut-off frequency of $f_1 = 800Hz$.

4.6. Upper-mid / tweeter cut-off frequency

The same approach has been applied to find the upper-mid / tweeter cut-off frequency and leads to a frequency $f_2 = 4500Hz$.

4.7. Choice of filter slopes

The choice of filter slopes is of extrem importance. It is necessary to observe carefully the shape of each transducer frequency response where the cut-off frequency will take place. A bad choice of the filter slopes can result in serious accidents on the loudspeaker system response. Additionally, in the case of the upper-mid / tweeters, it is not recommended to use soft slope filters close to the resonance frequency. This causes an important irregularity of the loudspeaker response.

In order to reduce to the minimum the overlap bands, Bairdand [6] and Lipshitz [7] advise the use of high slope crossover filters. In the following, we will show that such a strategy is badly adapted to co-axial loudspeakers and that it can generate undesirable directivity accidents. In addition, at low frequencies, the synthesis of these filters with transverse linear phase structures requires a rather high order that must rather remain reasonable for real-time implementation on DSP.

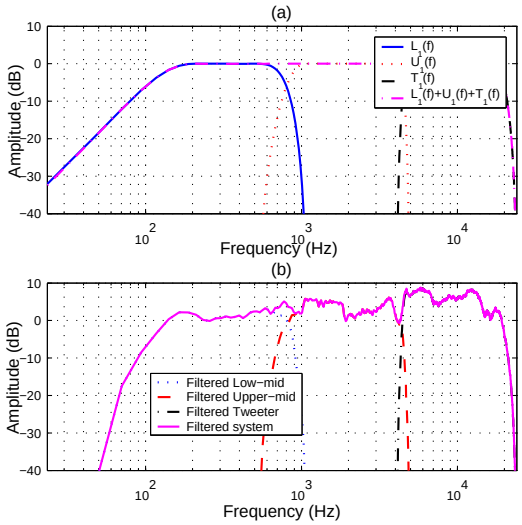

Fig. 7: Crossover 1 : (a) crossover filter frequency responses, (b) filtered co-axial source on-axis

In the following, we will maintain fixed the cut-off frequencies of the crossover filters ($800Hz$ and $4500Hz$) and we will investigate the influence of the filter slopes over the directivity and the radiation pattern of the three-way co-axial loudspeaker. We will distinguish the case of high slope filters (generally recommended for this type of application [6] and [7]) and the case of soft slope filters acting on a larger overlap band.

4.7.1. High slope filters

Table 1 summarizes the characteristics of a high slope crossover network called crossover 1.

Filter	$L_0(z)$	$U_0(z)$	$T_0(z)$
High-pass slope(dB/oct)	12	70	70
Low-pass slope(dB/oct)	70	70	48
Order	1101	501	221

Table 1: Crossover 1 characteristics

Figure 7-(a) illustrated the frequency response of the crossover 1 filters. In addition, the filtered transducers are well separated with very reduced overlap bands as shown by figure 7-(b).

Figure 8 shows the radiation pattern of the filtered

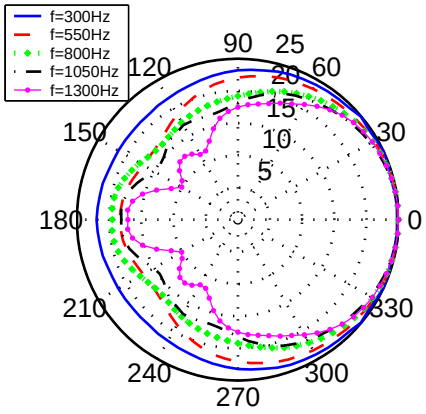

Fig. 8: Radiation pattern of the filtered (crossover 1) co-axial system over the Low-mid / Upper-mid overlap band

system over the Low-mid / Upper-mid overlap band. It appears that over this band, the two transducers ensure an homogeneous radiation without accidents. However, this is far from being the case of the Upper-mid / Tweeter overlap band given by figure 9. Indeed, over this band, the radiation pattern shows irregular fluctuations toward frequency.

Figure 10 gives an illustration of the problem by displaying the directivity index of the loudspeaker system versus frequency. Indeed, at $4000Hz$, the directivity of the system is mainly due to the directivity of the upper-mid driver and reaches a $12dB$ of directivity index. On the opposite, at $5000Hz$ the system tends toward a quasi-omnidirectional system (with a $DI = 6dB$). This is due to the fact that the tweeter contributes more to the radiated sound field and has a nearly omnidirectional pattern. As a result, high slopes crossover lead to fast and undesirable fluctuations of the directivity index on the overlap band.

4.7.2. Soft slope filters

We will now relax the high slope filters constraint by replacing the crossover 1 by a moderate slope filters characterized in table 2.

The overlap bands allowed by the new crossover are much wider as described on figure 11-(a) and 11-(b). From figures 12, 13 and 14, it can be inferred that

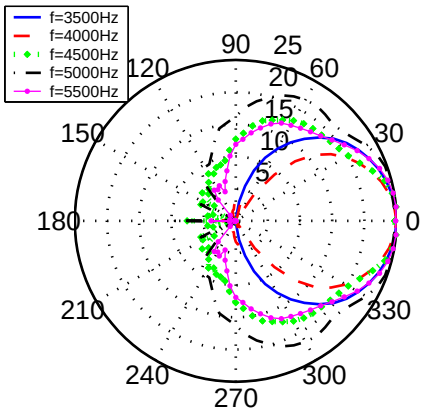

Fig. 9: Radiation pattern of the filtered (crossover 1) co-axial system over the Upper-mid / Tweeter overlap band

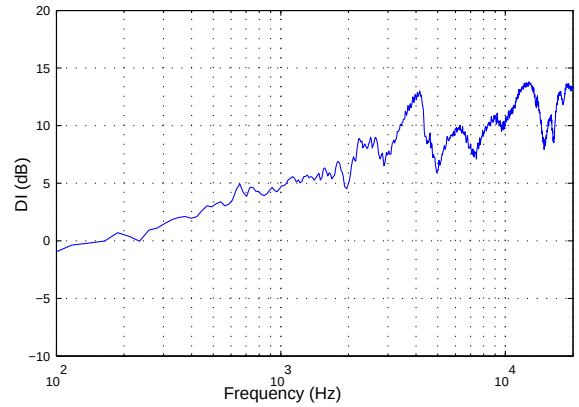

Fig. 10: Directivity index of the filtered (crossover 1) co-axial system

Filter	$L_0(z)$	$U_0(z)$	$T_0(z)$
High-pass slope(dB/oct)	12	18	12
Low-pass slope(dB/oct)	18	12	48
Order	801	137	39

Table 2: Crossover 2 characteristics

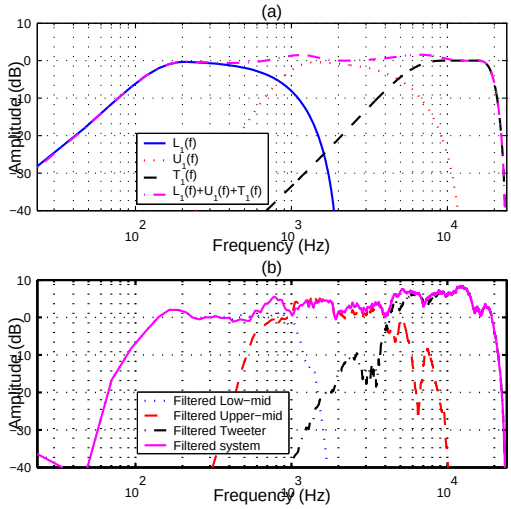

Fig. 11: Crossover 2: (a) crossover filter frequency responses, (b) filtered co-axial source

filter slopes have nearly no influence on the directivity of the system over the low-mid / upper-mid overlap band. However, the directivity of the source over the upper-mid / tweeter overlap band is more regular with this filtering.

4.7.3. Discussions

Let d_{um}^{eq}, be the equivalent diameter of the upper-mid radiating ring given by:

$$d_{um}^{eq} = \sqrt{(d_{um}^{o})^2 - (d_{um}^{i})^2} = 96mm \qquad (9)$$

The same approach is used to obtain the equivalent Low-mid diameter d_{lm}^{eq} given by equation (10):

$$d_{lm}^{eq} = \sqrt{(d_{lm}^{o})^2 - (d_{lm}^{i})^2} = 162mm \qquad (10)$$

The ratio of the low-mid / upper-mid, transducer dimensions is equal to $d_{lm}^{eq}/d_{um}^{eq} = 1.7$. However,

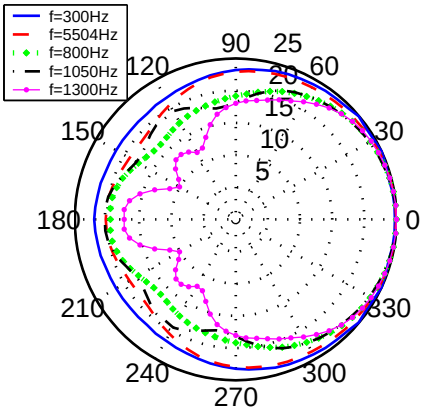

Fig. 12: Radiation pattern of the filtered (crossover 2) co-axial system over the Low-mid / Upper-mid overlap band

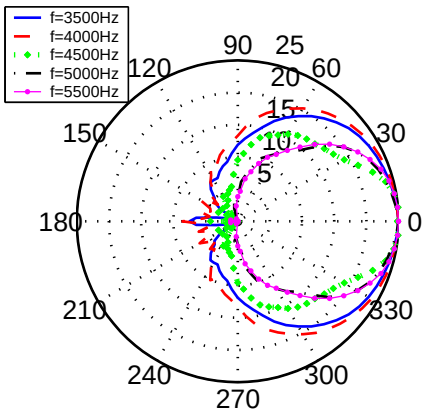

Fig. 13: Radiation pattern of the filtered (crossover 2) co-axial system over the Upper-mid / Tweeter overlap band

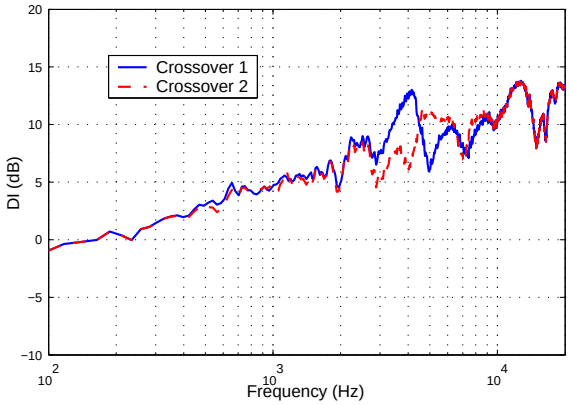

Fig. 14: Directivity index of the filtered (crossover 2) co-axial system

for the upper-mid / tweeter the ratio is $d_{um}^{eq}/d_{tw} = 3.4$. The transducers directivity over the low-mid / upper-mid overlap band are quite similar. However, it's not the case of the second overlap band since the upper-mid driver is nearly 4 times larger. As a result, special care should be taken when choosing crossover filter slopes in order to avoid serious directivity discontinuities.

When two adjacent transducers have rather different directivity, it is recommended to use soft slope filters. That makes it possible to widen the overlap band by ensuring a better compensation of the directivity differences.

Another fact that is not less important than the previously explained one is the filter bank complexity. Indeed, according to tables 1 and 2, the complexity of the implementation is reduced to the half with crossover 2 which will be retained for the simulations and experimental results of the following sections.

The correction of axial delays and a good choice of the crossover filter allow a noticeable improvement of the sound field radiated by the proposed co-axial loudspeaker system. However, some irregularities, especially due to directivity differences (over the upper-mid/tweeter overlap band), still occurred. In order to reduce such accidents, a new signal processing algorithm based on the optimization of the crossover transfer functions will be described in the next section.

5. OPTIMIZATION OF THE DIGITAL CROSSOVER

5.1. State of the art

The fluctuations on the radiation pattern and directivity index encountered over the upper-mid / tweeter overlap band are sometimes unacceptable (figures 13 and 14). Therefore, it is necessary to think about an optimization routine that reduces that defects. The idea thus would be to reconsider the overlap band (upper-mid / tweeter for the studied system) and try to seek the real or complex weighting to apply to each transducer in order to satisfy some optimization criteria.

5.2. Theoretical approach

Since around the first cut-off frequency there's no significant directivity accidents, the optimization process will focus on the upper-mid / tweeter overlap band. For this reason, the low-mid driver variables will not be included in the following formulas.

Let A_i and B, be the vectors given by:

$$A_i = [H_{um}(r,\theta_i,f)U_1(f)\ H_{um}(r,\theta_i,f)T_1(f)]^T$$
$$B = [W_{um}(f)\ W_{tw}(f)]^T \quad (11)$$

A_i is the vector containing the filtered system transfer functions measured at the listening point $M(r,\theta_i)$ and relative to the frequency f. $W_{um}(f)$ and $W_{tw}(f)$ are the frequency weights to be applied to the upper-mid and the tweeter device.

In order to force given directions θ_i, $i = 1.N$ of the radiation pattern to fixed gains g_i, we have to solve the following linear system:

$$C^H B = G \quad (12)$$

In this equation, $(.)^H$ denotes the complex conjugate transpose operator. C and G are given by:

$$C = [A_1 ... A_N]^T$$
$$G = [g_1 ... g_N]^T \quad (13)$$

The least squares solution of the linear system of equation 12 is obtained by minimizing the cost $J_0 = |C^H B - G|^2$ with respect to B, [?] and is equal to:

$$B_{opt} = (CC^H)^{-1}CG \quad (14)$$

In the cost function J_0, the absolute phase of the vector G is difficult to estimate (propagation delay + system group delay). This term is generally not taken into account and a desired diagram is given only by the desired amplitudes. This approach is legitimate since the user, is interested only to the amplitude of the field radiated by the source in various directions. The cost function can then be written:

$$J_1(B) = \sum_{i=1}^{N}(|A_i^H B| - |g_i|)^2 \quad (15)$$

The control of the radiation pattern requires to fix a target diagram in all the desired directions and over all the frequencies of the overlap band. Using the previous equations, we can write the directivity index of the filtered system as follow:

$$DI = 10log10(\frac{2}{\int_0^\pi \frac{|A_i^H B|^2}{|A_0^H B|^2} sin(\theta)d\theta})$$
$$= 10log10(\frac{B^H D B}{B^H E B}) \quad (16)$$

where $E = 2A_0 A_0^H$ and $D = \int_0^\pi A_i A_i^H sin(\theta)d\theta$.

5.3. Formulation of the optimization problem

In a multi-way loudspeaker system, it is suitable to achieve regular directivity index over the overlap bands. This criterion cannot be obtained with conventional discreetly distributed transducers because of the phase cancellation problems. However, using co-axial loudspeakers combined with dedicated signal processing techniques, one could satisfy the previous target.

In a co-axial loudspeaker system, no lobbing occurs on the overlap bands and a regular directivity index is equivalent to a homogeneous radiation pattern that narrowed when the frequency increases. This was the case of the low-mid / upper-mid overlap

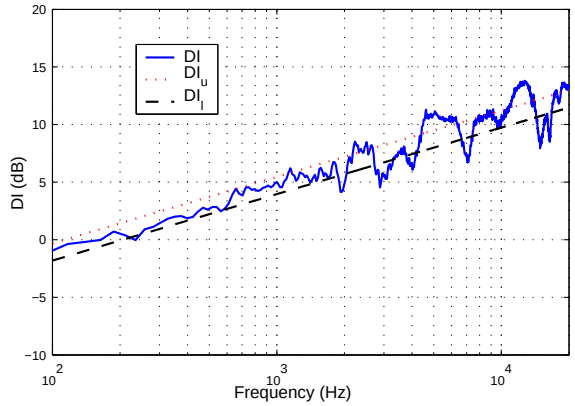

Fig. 15: Directivity index and target interval

band given by figures 12 and 14. However, over the upper-mid / tweeter overlap band, small DI irregularities still remain and induce consequent radiation fluctuations as can be seen from figure 13.

The principle of the optimization consists in finding the vector B minimizing the square form J_1 (equation 15) of the error between the corrected system radiation pattern and a desired target fixed in advance. This optimization should satisfy the following constraints:

5.3.1. Directivity index constraint

Let DI_{av} be the first order polynomial which approaches the directivity index of the filtered system over the low-mid / upper mid overlap band. An easy way to correct the residual directivity fluctuations over the upper-mid / tweeter overlap band, is to force the directivity index of the filtered system to lie within two straight lines $DI_l = DI_{av} - \delta/2$ and $DI_u = DI_{av} + \delta/2$. δ is a parameter defining the width of the fluctuation interval. Figure 15 summarizes the previous description.

The directivity index of equation 16 must so satisfy:

$$DI_l \leq 10log10(\frac{B^H E B}{B^H D B}) \leq DI_u \qquad (17)$$

This equation can be considered as two independent constraints given by:

$$\begin{aligned} B^H(E-\alpha D)B \leq 0 \\ B^H(D-\beta E)B \leq 0 \end{aligned} \qquad (18)$$

with $\alpha = e^{\frac{DI_u Log(10)}{10}}$ and $\beta = e^{\frac{DI_l Log(10)}{10}}$

5.3.2. Saturation and filter design constraints

In order to avoid power amplifiers saturation and hard filter synthesis with reasonable order, the amplitude of the weights W_{um} and W_{tw} must be maintained inside a given interval $[\varrho, \rho]$. Analytically, this constraint can be written:

$$\begin{aligned} \varrho \leq B^H I_1 B \leq \rho \\ \varrho \leq B^H I_2 B \leq \rho \end{aligned} \qquad (19)$$

Were I_1 and I_2 are two matrix defined by:

$$I_1 = \begin{pmatrix} 1 & 0 \\ 0 & 0 \end{pmatrix}$$

and

$$I_2 = \begin{pmatrix} 0 & 0 \\ 0 & 1 \end{pmatrix}$$

5.4. Optimization procedure

The optimization problem can be written:

$$(P): \begin{cases} \min_B(J_1(B)) \\ \text{subject to} \\ B^H(E-\alpha D)B \leq 0 \\ B^H(D-\beta E)B \leq 0 \\ \varrho \leq B^H I_1 B \leq \rho \\ \varrho \leq B^H I_2 B \leq \rho \end{cases}$$

The size of the unknown vector B is equal to 2. Thus, a systematic approach could be used to solve the problem P. It consists in sampling the amplitude: $[\varrho, \rho]$ and phase: $[-\pi, \pi]$ intervals allowed for the components of the vector B. The algorithm searches for all the couples (W_{um}^k, W_{tw}^k) satisfying the several constraints (directivity and saturation).

Finally, we select the couple minimizing the cost $J_1(B)$ of equation 15.

In order to reduce the complexity of the problem (P), the W_{um} weight will be fixed to unity. Thus, only the tweeter weight W_{tw} will be the parameter to be optimize. This approach is justified since the directivity defects encountered on the overlap band are due to frequency (amplitude and phase) shifts between the filtered transducer transfer functions (components of the vector A_i). This will also relax the design of the new crossover network since only the tweeter filter $T_1(z)$ will be modified.

5.5. Experimental results

The optimization routine will now be applied to enhance the control of the system directivity over the $[2250Hz, 6750Hz]$ overlap band. The parameters used are $\delta = 1.5dB$, $\varrho = 0.25$ and $\rho = 4$. The cost function to be minimized is given by :

$$J_1(B) = (|A_1^H B| - 1)^2 \qquad (20)$$

A_1 contains the filtered transducer transfer functions relative to $\theta = 0$. This cost reduces axial deviations on the filtered system frequency response over the considered overlap band.

5.5.1. Case of positive real weights

In a first step, we consider just one degree of freedom that is the amplitude of the weights W_{tw}. Figure 16 and 17 show the radiation pattern and the directivity index of the optimized system in this case. From these figures, we can conclude that real weights could not achieve the desired requirements especially in term of directivity index. This result is not surprising since as stated before, the directivity accidents over the overlap band are due to amplitude and phase shifts.

5.5.2. Case of complex weights

A noticeable improvement can be obtained when allowing two degree, of freedom (amplitude and phase) as can be seen from figure 19. However, serious radiation accident occur at the cut-off frequency $f_2 4500Hz$ (figure 18). In order to counteract this problem, we should have better control on the radiation pattern by taking into account other directions

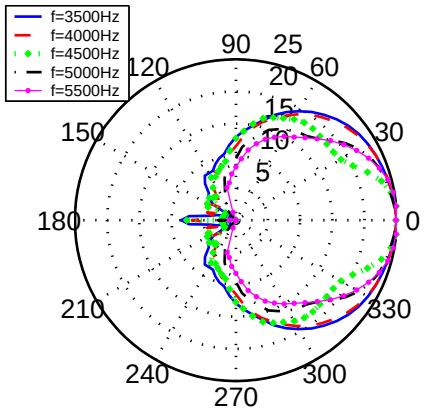

Fig. 16: Radiation pattern of the optimized system using real weights

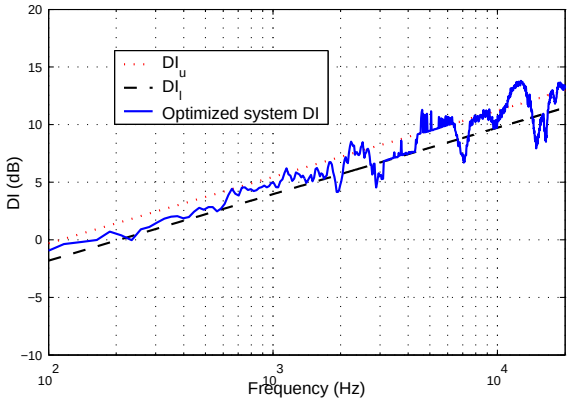

Fig. 17: Directivity index of the optimized system using real weights

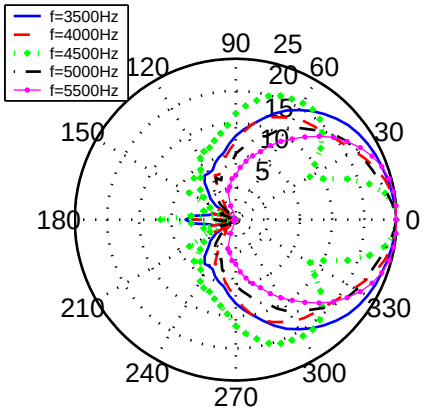

Fig. 18: Radiation pattern of the optimized system using complex weights

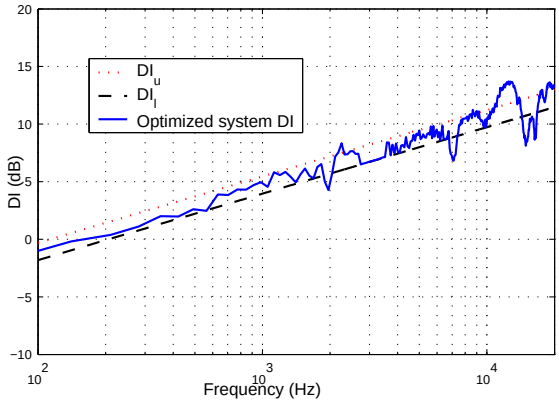

Fig. 19: Directivity index of the optimized system using complex weights

in the function $J_1(B)$. This cost, will now be modified to fix the beam width at $-3dB$ to 30°. The new cost function is given by:

$$J_1(B) = (|A_1^H B| - 1)^2 + (|A_2^H B| - \sqrt{2})^2 \qquad (21)$$

where A_2 contains the filtered transducer transfer functions at 30°. The results obtained are given by figures 20 and 21. We notice that It can be noticed that the directivity irregularity has disappeared at $4500Hz$ and the directivity pattern remains very similar to nearby frequencies. Additionally, over the $[2250Hz, 6750Hz]$ overlap band, the DI is well constrained inside the gage targeted.

The frequency responses of the optimized system at 0° and 30° are given by figure 22. From this figure, we can see a homogeneous and smooth polar decrease. However, additional signal processing must be carried in order to equalize the system response on-axis or over a given solid angle.

5.6. Design of the optimized crossover network

As stated in section 5.4, during the optimization procedure only the tweeter filter $T_1(f)$ will be modified to $T_{opt}(f)$ given by:

$$T_{opt}(f) = T_1(f) W_{tw}(f) \qquad (22)$$

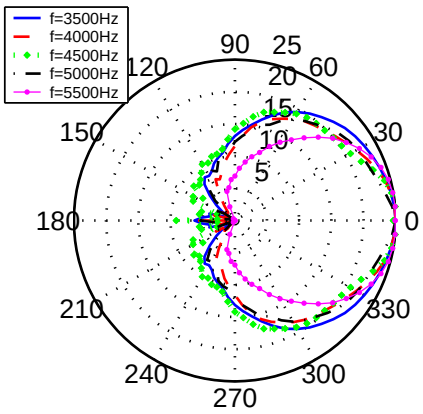

Fig. 20: Radiation pattern of the optimized system

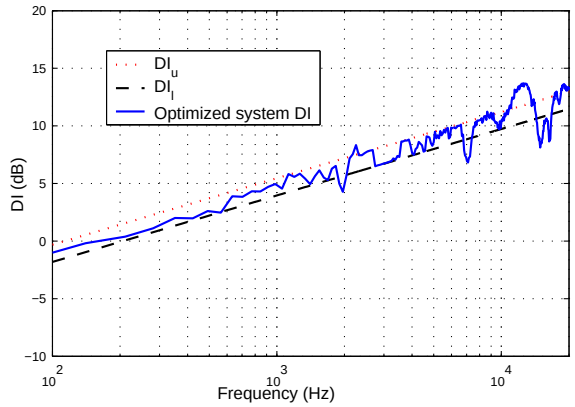

Fig. 21: Directivity index of the optimized system

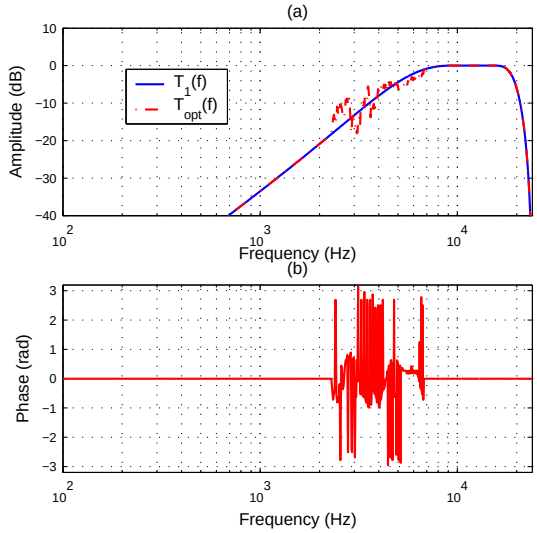

Fig. 23: Tweeter responses: (a) Amplitude responses (b) Phase shift between the original and the optimized filter

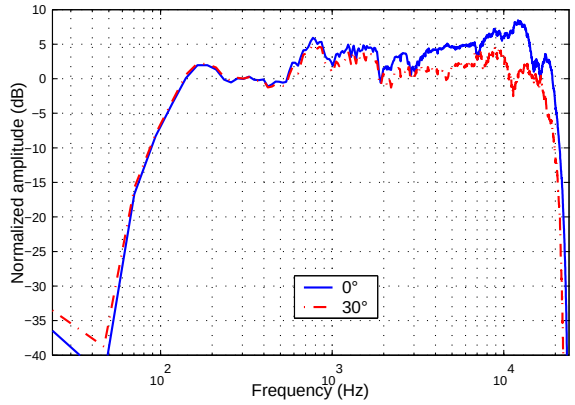

Fig. 22: Optimized system responses

The amplitude of the initial and the new tweeter filter are given by figure 23-(a). They are identical except on the cut-off band where the amplitude of the optimized filter fluctuates around the original band-pass filter. In figure 23-(b), we show the phase shift between the two transfer functions. The phase of the tweeter filter is not linear after optimization due to the complex weights $W_t w(f)$ applied on the overlap band.

The impulse response $t_{opt}n$ of the new tweeter filter will then be obtained using the generalized least squares method [10].

The transfer function of the optimized system measured in a point $M(r,\theta)$ of the space becomes then:

$$H_{opt}(r,\theta,f) = H_{lm}(r,\theta,f)L_1(f)$$

$$+H_{um}(r,\theta,f)U_1(f) + H_{tw}(r,\theta,f)T_{opt}(f) \qquad (23)$$

6. EQUALIZATION

Many techniques can be used to equalize the loudspeaker response [11], [12]. The method proposed

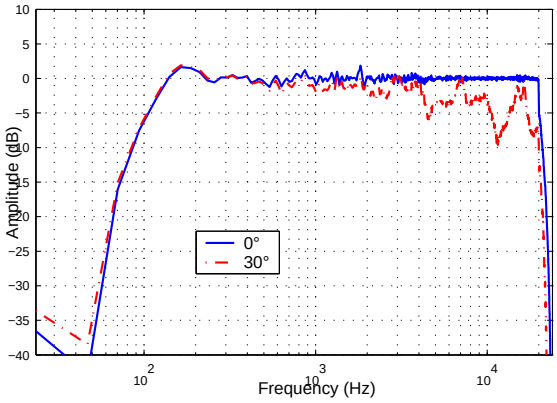

Fig. 24: On-axis equalized loudspeaker system

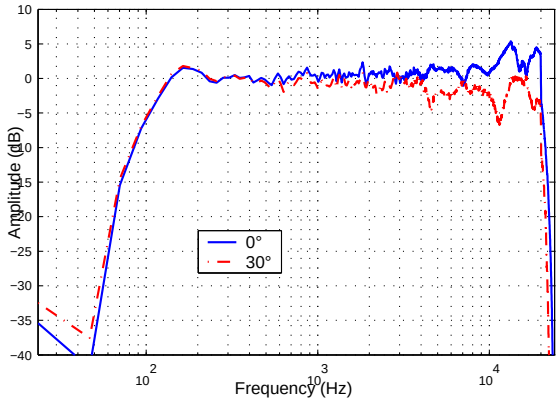

Fig. 25: Average multi-points equalization of the loudspeaker system

here is based on spectral inversion of the system response. Let $L(f)$ be the frequency response to be corrected. The equalizer target response $E(f)$ is given by:

$$E(f) = \begin{cases} \dfrac{1}{L(f)} & \text{if } f \in [f_l, f_u] \\ 1 & \text{else} \end{cases} \qquad (24)$$

were $[f_l, f_u]$ is the equalization band-width fixed to $[100Hz, 20kHz]$ for the three-ways co-axial loudspeaker system.

Applying the frequency sampling method to $|E(f)|$ [13], we obtain the impulse response of the linear phase amplitude equalizer to be implemented on the DSP device.

6.1. On-axis equalization

This equalization is relative to the single listening point where measurements were performed ($L(f) = H_{opt}(r, 0, f)$. In the case of a co-axial loudspeaker system, driver's physical distribution erases the amplitude cancellation problem around crossover frequencies. As a result, the source response remains quite regular to up $4000Hz$ when the listener moves to up 30 degrees out of axis. Simulation results are given by figure 24 for an equalizer of order 700.

6.2. Average multi-points equalization

As the frequency increase, the tweeter diameter d_{tw} starts to be equivalent to the wave lengths to be reproduced. As a result, quick decrease of the system response over the high frequency band can be seen when moving out off axis. Better results can be achieved with an average multi-points equalization of the system response over a given solid angle. The response to be equalized is thus the average of several frequency responses measured over a given solid angle θ_K. This response is given by:

$$L(f) = \frac{1}{K} \sum_{i=1}^{K} H_{opt}(r, \theta_i, f) \qquad (25)$$

An example of this correction over a 30° solid angle is shown by figure 25. We can notice that the low-mid / upper-mid frequency band of the equalized system response is very close to that obtained with on-axis equalization case. However, a noticeable high-frequencies boost is achieved with the average multi-points equalization and leads to a better signal reproduction than the classical equalization technique.

7. REAL-TIME IMPLEMENTATION OF THE DIGITAL FILTER BANK

The axial delays compensation, the linear phase crossover filter bank and the loudspeaker equalizer was then implemented on a digital signal processor. Practical constraint and trade-offs of a real-time application will be discussed in the following.

7.1. DSP implementation issues

The DSP board includes the $ADSP-21262$ device operating at $200MHz$ (800MFLOPS). This processor integrates $2Mbits$ of on-chip dual ported SRAM and $4Mbits$ of mask-programmable ROM. This high level of on-chip memory enables sustained DSP and I/O performance, without the need for external memory.

The bloc diagram of the audio scheme is given by figure 26. First, the DSP convolves the input sequence with the equalizer impulse response. Then, the input sequence of each band-pass filter is updated. Finally, the 21262 computes the sample to be sent to each DAC after convolution of the updated delay line with the impulse response of the relative band-pass filter. The implementation of the filter bank was done using the assembly language in order to overcome standard code optimization problems.

7.2. System performance and experimental results

At $48kHz$ sampling frequency, the real-time constraint is equal to $20,8\mu s$ which is equivalent to 4167 DSP cycle. Table 3 summarizes filter orders and the average number of DSP cycles required to perform the different signal processing functions. The digital filter bank accounts for 57.6% of the total real-time constraint.

The implementation has a code size of $176Kbits$ and uses a 4855 word of data (1 word = 32 bits). These values are fully compatible with the $2Mbits$ RAM available on the 21262 DSP.

Function	Filter order	Cycle number
Equalizer	701	716
Low-mid filter	811	824
High-mid filter	165	177
Tweeter filter	680	691
Total	2347	2398

Table 3: Average number of DSP cycles per function

Figure 27, 28 and 29 show the results of the measured system in an anechoic room. The floating-point implementation of the digital filter bank exhibits slight performance degradation in comparison with simulations given in the previous sections.

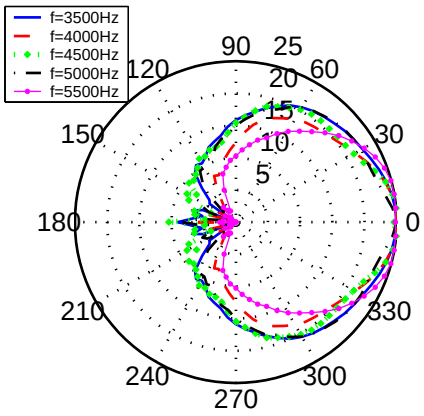

Fig. 27: Measured radiation pattern of the optimized system

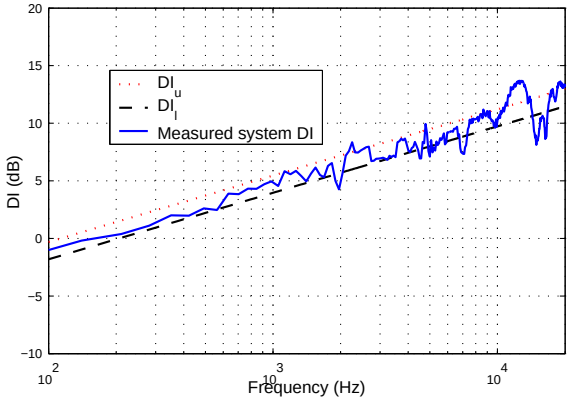

Fig. 28: Measured directivity index of the optimized system

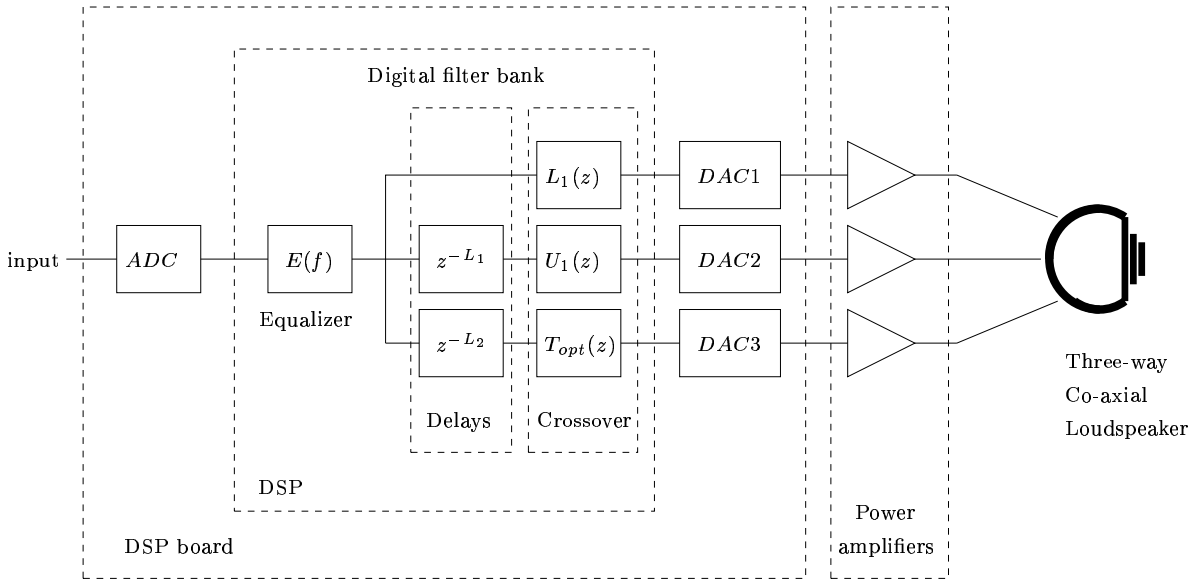

Fig. 26: Block diagram of the audio scheme

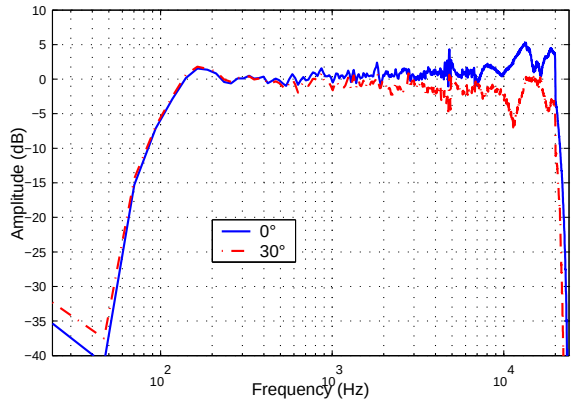

Fig. 29: Measured responses of the optimized loudspeaker system with average multi-points equalization over 30 degrees

Some A/B tests made to compare a passively filtered realization of the system to the digitally filtered one are in progress. The first informal results confirm that the optimized co-axial loudspeaker have a more localized stereo image and better tonal neutrality achieved by the equalizer. The proposed directivity control also achieves a large and stable sweet-spot.

8. CONCLUSIONS AND FUTURE WORKS

8.1. CONCLUSIONS

The digital control of the sound field radiated by a practical co-axial source has been investigated. The impact of the time shift correction, crossover type and slope on the directivity index and polar pattern versus frequency has been described. The insights provides on the matter have revealed some remaining imperfect behaviors. As a result, a new approach has been proposed consisting of an optimization algorithm providing extra degree of freedom. The conjunction of a real time implementation of this technique especially designed for a three-way co-axial driver achieves a nearly ideal acoustic source.

8.2. FUTURE WORKS

Recently, the three-way co-axial loudspeaker, introduced in [1], has been extended to an innovative

four-way system able to reproduce the entire audio frequency band. The use of the signal processing technique addressed in this paper on the framework of the new four-ways co-axial loudspeaker is currently in progress.

9. APPENDIX

Given the amplitude $P(r,\theta,f)$ of the pressure in the far field, the total radiated power is obtained by integrating the intensity over a sphere enclosing the source,

$$\wp(f) = \frac{1}{2\rho_0 c}\int_{4\pi} P^2(r,\theta,f)r^2 d\Omega \qquad (26)$$

Recalling that $P(r,\theta,f) = F(\theta,f)P_{ax}(r,f)$ (equation 5) and noting that r is constraint for the integration, we can write:

$$\wp(f) = \frac{1}{2\rho_0 c}r^2 P_{ax}^2(r,f)\int_{4\pi} F^2(\theta,f)d\Omega \qquad (27)$$

For a simple source that generates the same acoustic power, the pressure amplitude $P_s(r,f)$ to be found at the distance r is given by

$$\wp(f) = \frac{4\pi r^2 P_s^2(r,f)}{2\rho_0 c} \qquad (28)$$

The ration of these intensities reveals how much more-efficiently a directional source concentrates the available acoustic power into a preferred direction. This ratio defines the directivity $D(f)$ as

$$D(f) = \frac{I_{ax}(r,f)}{I_s(r,f)} = \frac{P_{ax}^2(r,f)}{P_s^2(r,f)} \qquad (29)$$

Substitution of 27 and 28 into 29 results in

$$D(f) = \frac{4\pi}{\int_{4\pi} F^2(\theta,f)d\Omega} \qquad (30)$$

Due to the axis-symmetry of the co-axial loudspeaker system, the incremental solid angle $d\Omega$ is equal to $2\pi sin(\theta)d\theta$. The directivity of the system is thus determined from the directional function $F(\theta,f)$ by

$$D(f) = \frac{2}{\int_{4\pi}(F(\theta,f))^2 sin(\theta)d\theta} \qquad (31)$$

10. REFERENCES

[1] B. Debail and H. Shaiek, "Radiated sound field analysis of loudspeaker systems: discrete geometrical distribution of anular membranes versus co-incident annular rings", *119th convention of the AES*, New York, Oct 2005.

[2] D.S. Fink, "Time Offset and Crossover Design", *J.AES*, Vol 28, N9, Sep 1980.

[3] R. Bews, "Digital crossover networks for active loudspeaker systems" ,*Ph.D. dissertation*, University of Essex, 1987.

[4] S.H. Linkwitz, "Active crossover networks for non-coincident drivers", *J.AES*, Vol 24, N1, Jan/Feb 1979.

[5] L E. Kinsler et al, "Fundamentals of Acoustics", *John Wiley and sons*, Fourth edition, 2000.

[6] J. Bairdand and D. Mcgrath, "Practical application of linear phase crossovers with transient bands approaching a break wall responses for optimal loudspeaker frequency, impulse and polar responses", *115th convention of the AES*, Oct 2003.

[7] S.P. Lipshitz and J. Vanderskoy, "A family of linear-phase crossover networks of high slopes derived by time delay", *J.AES*, Vol 31, pp 2-20, Jan/Feb 1983.

[8] H. Shaiek, "Configuration automatique d'enceinte pour le "Home Cinema"" , *Technical report*, Cabasse-ENST Bretagne, jul 2003.

[9] R. Lamberti "Apercu sur les méthodes de filtrage des réseaux d'antenne", *Cours INT*, 3éme année, 1996.

[10] T.I. Laakso et al "Splitting the time delay", *IEEE Signal Processing Magazine*, pp 30-60, Jan 1996.

[11] G. Ramos et al, "Direct method with random optimization for loudspeaker equalization using IIR parametric filters", *ICASSP*, pp 97-100, May 2004.

[12] R. Greenfield and M.O. Hawksford, "Efficient filter design for loudspeaker equalization", *JAES*, vol 39, no 10, pp 739-751, Oct 1991.

[13] IEEE, "Programs for Digital Signal Processing", *IEEE Press*, John Wiley & Sons, 1979.

[14] L. Jackson, "Digital filter design", *Van Nostrand*, New York, 1982.